Correlated motions of two hydrodynamically coupled particles confined in separate quadratic potential wells

L. A. Hough and H. D. Ou-Yang
Department of Physics, Lehigh University, Bethlehem, Pennsylvania 18015
(Received 12 June 2001; published 18 January 2002)

We report a study of the correlated motions of two hydrodynamically coupled colloidal particles, each of which is trapped in a quadratic potential well defined by optical tweezers (optical traps). By setting one of the trapped particles into forced oscillation using oscillating optical tweezers, we measure the displacement and phase shift of each of the particles over a wide frequency range. From the in-phase and out-of-phase motions of both of the particles in the traps, we determine the correlated motions of the coupled mechanical system as a function of frequency. A theoretical model is developed to calculate the response tensor of the coupled mechanical system. The experimental results are in agreement with the prediction of the theoretical model. This method may be extended to more general applications, such as the investigation of the micromechanical properties of viscoelastic and/or heterogeneous media.

DOI: 10.1103/PhysRevE.65.021906 PACS number(s): 87.80.Cc, 83.10.Pp, 82.70.Dd, 83.85.Vb

I. INTRODUCTION

Colloids, polymer solutions, microemulsions, and biological cells and tissues are intrinsically complex. The complexity arises from two factors: interactions between the constituents, and the structural heterogeneity of the material (which occurs in a broad range of length scales). As a result of the interplay between the interactions and structural heterogeneity, these systems often reveal rich dynamical responses in their mechanical properties over a wide range of frequencies. Because of the interest in the mechanical properties of these systems, various techniques have been developed to probe their dynamical behavior at the microscopic level. The remaining challenges are the predictions of the microscopic structures based on the microscopic viscoelastic properties of the system.

In a typical ''single particle microrheology'' study, thermal motions of Brownian particles [1–5], or forced oscillations of micron-sized probe particles [6–9], are used to determine the viscoelastic properties of soft materials around the probe particles. Based on hydrodynamic methods, the range of the probed materials extends to approximately one radius beyond the surface of the probe particle. Thus, the measured viscoelasticity will depend on the size of a probe particle if the scale of the material inhomogeneity is comparable to the particle size. Therefore, it is not surprising that results from single particle microheology studies sometimes differ from those obtained from conventional rheometers. Accordingly, one might expect the local viscoelastic properties to be comparable to the bulk viscoelastic properties only after averaging over an extended range of the material [5,6].

To put the problem in theoretical perspective, Levine and Lubensky showed that the longitudinal motions of two microscopic particles in local viscoelastic environments are coupled by the mean viscoelasticity of the material between the particles [10]. Along the same vein, Crocker *et al.* measured the ''distinct'' diffusion coefficient of colloidal pairs in guar and *F*-actin solutions and reconciled the difference between the microscopic and macroscopic viscoelasticities using ''two-point microrheology'' [5]. To further develop microrheology, it appears that the next logical step is to understand fundamentally how the viscoelasticity changes as the length scale between the probes is varied in a systematic way. The work described below provides the basis for a different methodology to study the mechanical properties in the microscopic environment of complex fluids.

In this paper, we present a study of the correlated motion of a pair of hydrodynamically coupled colloidal particles each held in a harmonic potential well. The distance between the potential wells can be varied such that many length scales can be explored. As a proof of principle, we choose a simple viscous medium in which the potential wells for the two particles are created by optical tweezers (optical traps). The fixed potential well created by the optical tweezers has the same effect as a frequency independent elastic medium around the particle. The measurements of the correlated motion of these two particles provide a test for a simplified viscoelastic model in which the motion of both of the probe particles can be completely described by a response tensor of the coupled mechanical system.

The experimental arrangement, shown in Fig. 1, is similar to that of Meiners and Quake [11]. However, instead of examining the temporal correlation functions of the two-particles' Brownian motions, we measure the phase and displacement amplitude of both of the particles in response to an external sinusoidal perturbation on one of the particles.

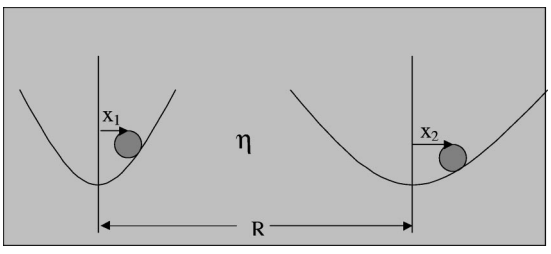

FIG. 1. Two colloidal particles move in two separate quadratic potential wells a distance R apart, in a simple liquid with viscosity η.

The amplitude and the phase shift of the particles' motions provide a complete description of the correlated motion. This approach provides advantages in both experimental ease and measurement sensitivity [12,13].

II. THEORY

To describe the motions of the particles, we seek to find a simple relation between the forces on the particles and the motions of the particles in terms of a response tensor. Specifically, $x_n(\omega)=\chi_{nm}(\omega)F_m(\omega)$, where x_n is the motion of the nth particle, F_m is the external force on the mth particle, χ_{nm} is the complex response tensor of the system, with n, $m=1$ or 2. In the case of a sinusoidal perturbation to one of the particles ($F_1=\text{const}, F_2=0$), the complex response tensor is simply related to the correlated in-phase and out-of-phase motions of the particles. Conversely, the measured phases and displacements of the two particles uniquely determine the elements of the response tensor.

To calculate the elements of the response tensor, we start with the coupled differential equations for two hydrodynamically coupled, identical, particles in two spatially separated quadratic potential wells [11,14].

$$\dot{x}_1(t)=H_{11}(-k_{\text{ot1}}x_1+f_1)+H_{12}(-k_{\text{ot2}}x_2+f_2),$$

$$\dot{x}_2(t)=H_{21}(-k_{\text{ot1}}x_1+f_1)+H_{22}(-k_{\text{ot2}}x_2+f_2), \qquad (1)$$

where

$$H_{11}=H_{22}=\frac{1}{6\pi\eta a}, \quad H_{12}=H_{21}=\frac{1}{4\pi\eta R} \qquad (2)$$

are the lowest order components, in $1/R$, of the Oseen Tensor [14] for motions in the longitudinal directions along the line between the centers of the two particles; k_{ot1} and k_{ot2} are the ''spring constants'' of the quadratic potential wells, a is the radius of each of the particles, $f_1(t)$ and $f_2(t)$ are the random Brownian forces, and η is the viscosity of the liquid. The center-to-center distance between the particles, R, is taken to be a constant because the experiments are carried out under the conditions of $R \gg x_1$ and $R \gg x_2$. Since we are dealing with low Reynolds number fluid motion, the inertial terms are neglected in Eq. (1).

Because most of the details are shown in the Appendix, we simply state that the elements of the response tensor are calculated in the following manner. The temporal autocorrelation and cross-correlation functions of the particles' positions are calculated from Eq. (1). The imaginary components of the response tensor are then calculated from the correlation functions by the fluctuation-dissipation theorem. The real parts of the response tensor are then determined from the imaginary parts by the Kramers-Kronig relation [15]. The elements of the response tensor are

$$\chi_{11}=\frac{1}{(s_+-s_-)k_{\text{ot1}}\tau}\left[\left(\frac{(\alpha+\tau s_+)s_+^2}{\omega^2+s_+^2}-\frac{(\alpha+\tau s_-)s_-^2}{\omega^2+s_-^2}\right)+i\left(\frac{(\alpha+\tau s_-)\omega s_-}{\omega^2+s_-^2}-\frac{(\alpha+\tau s_+)\omega s_+}{\omega^2+s_+^2}\right)\right], \qquad (3)$$

$$\chi_{12}=\chi_{21}=\frac{\epsilon}{(s_+-s_-)k_{\text{ot1}}\tau}\left[\left(\frac{s_-^2}{\omega^2+s_-^2}-\frac{s_+^2}{\omega^2+s_+^2}\right)+i\left(\frac{\omega s_+}{\omega^2+s_+^2}-\frac{\omega s_-}{\omega^2+s_-^2}\right)\right], \qquad (4)$$

$$\chi_{22}=\frac{1}{(s_+-s_-)k_{\text{ot1}}\alpha\tau}\left[\left(\frac{(1+\tau s_+)s_+^2}{\omega^2+s_+^2}-\frac{(1+\tau s_-)s_-^2}{\omega^2+s_-^2}\right)+i\left(\frac{(1+\tau s_-)\omega s_-}{\omega^2+s_-^2}-\frac{(1+\tau s_+)\omega s_+}{\omega^2+s_+^2}\right)\right], \qquad (5)$$

where s_- and s_+, the eigenvalues of the symmetric and antisymmetric modes, are the poles of the response tensor in the complex plane [15], and given by,

$$s_\pm=\frac{-(1+\alpha)\pm\sqrt{(1-\alpha)^2+4\alpha\epsilon^2}}{2\tau}, \qquad (6)$$

where $\alpha=k_{\text{ot2}}/k_{\text{ot1}}$, $\epsilon=H_{12}/H_{11}$, and $\tau=1/(k_{\text{ot1}}H_{11})$. The response tensor is symmetric, however, since the potential wells are not equal, in general, neither are the diagonal response elements.

III. EXPERIMENT

The experimental arrangement, shown in Fig. 2, consists of two optical tweezers formed by focusing two independently steered, perpendicularly polarized laser beams ($\lambda=532$ nm. Spectra Physics, Millenia Nd:YVO_4) using a microscope objective (Olympus, UPlanApo 100× NA 1.35) in an inverted microscope (Olympus IX-70). Splitting the laser beam with a polarizing beam splitter (PBS1) creates two beams. The first laser beam, P polarized and steered by a homemade piezocontrolled mirror, $M2$ (Physik Instrumente, $P830$-40), forms the stationary optical tweezers. The second laser beam, S polarized, is steered by a high frequency piezodriven mirror, $M1$ (Physik Instrumente, PI-$S224$), and forms the oscillating optical tweezers. A sinusoidal signal created by a Stanford research systems frequency synthesizer (SRS DS-345) is fed in a piezoelectric driver (Physik Instrumente, $P863$) to drive the steering mirror. The two beams recombine at the polarizing beam splitter PBS2 before going into the microscope. By adjusting the mirror, $M2$, the separation of the two beams can be varied.

A CCD (MT1 CCD 72) camera is used to generate a video image of the trapped particle for optical alignment and determination of interparticle distance (Global lab Image Software and DT3155 Frame Grabber, both from Data Translations). The forward scattering intensity from each beam is separately detected by the split photodiode, PD (Hamamatsu $S4204$). The output electrical current signal from the PD is

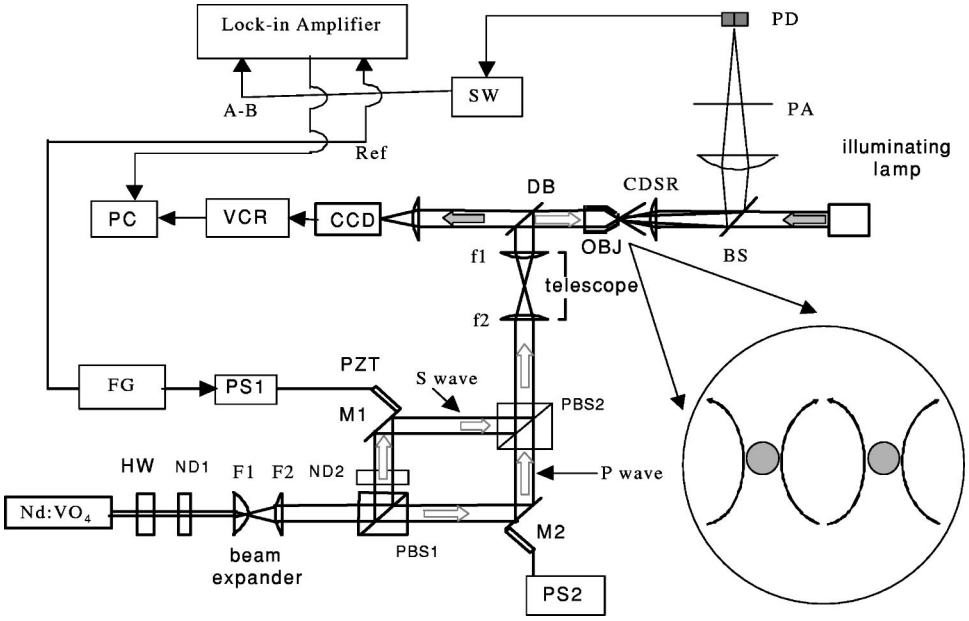

FIG. 2. A schematic of the dual-tweezers setup. HW is a half-wave plate, ND, neutral density filter, PBS, polarizing beam splitter, $M1$ and $M2$ are piezocontrolled mirrors, PS, piezopower supply, DB dichroic mirror to allow the laser beam to reflect and long wavelength illuminating light to pass, and PA is the polarization analyzer. The second piezocontrolled mirror $M2$ is kept stationary for the two-particle experiments, and can oscillate for calibrating the spring constant of the P wave trap. In the diagram, the sample is located immediately to the right of the objective lens OBJ.

fed into a lock-in amplifier (Stanford Research, SR830), and the reference signal is taken from the frequency synthesizer (SRS DS-345), that is, also used to drive the oscillating mirror $M1$. In this arrangement, the lock-in amplifier measures the magnitude and the phase shift of the signal from the photodiode detector, where the measured phase shift is relative to that of the driving signal. The forward scattering of the laser beam diffracted by a silica particle fixed at the cover glass is used to establish the reference for determining the frequency dependence of the steering mirror's displacement and phase shift. From the phase shift of the oscillating mirror motion and that of the moving particle, both relative to the signal of the function generator, we obtain the phase shift of the moving particle relative to that of the oscillating tweezers [13].

The telescope, composed of the lens pair $f1$-$f2$, is arranged such that the location of $M1$ and $M2$ are conjugate to the back focal plane of the objective. Thus, any rotational motion of the laser beams due to $M1$ or $M2$ is pivoted at the back focal plane of the objective lens. The positions of $M1$ and $M2$ are important to ensure that the laser intensity remains approximately constant when the laser beam oscillates laterally at the focal plane of the microscope objective lens. Furthermore, the split PD is located at the plane conjugate to the focal plane of the objective so that the rotational motion of the tweezers produces a rotational motion of laser beam that is pivoted at the surface of the PD. The proper location of the PD can be found by moving the PD along the optical axis near the calculated conjugate plan until no signal (less than 1% compared to that of the signal with a trapped particle in motion) can be detected at the oscillating frequency of $M1$ in the absence of a particle in the trap.

The precise positioning of the PD is necessary to guarantee that the signal detected by the PD is purely due to the lateral translation motion of particle relative to that of the laser tweezers. Since the laser tweezers are oscillating sinusoidally, the PD signal is measured relative to a moving reference frame, not to the rest laboratory frame [13]. A straightforward transformation is used to obtain the motion in the stationary lab frame from the motion determined by the lock-in amplifier from the PD signal in the moving reference frame (details of which are given in the following section).

To ensure that no other particles are present in the vicinity of the particle under investigation, a dilute aqueous suspension of 1.6-μm diameter silica spheres (Duke Scientific, Palo Alto, California) is placed in a flow cell. An individual sphere is isolated in each of the optical traps, and filtered deionized water flushes away the excess particles.

IV. EXPERIMENTAL RESULTS

To determine the spring constant, k_{ot}, of an optical trap, a particle is trapped in an oscillating optical trap that moves perpendicular to the optical axis with a displacement described by $A\cos(\omega t)$ where A is the amplitude of the trap and ω is the angular frequency. Since the system has low Reynolds number, mathematically, a damped harmonic oscillator without the inertia term describes the problem. It can be shown readily that the particle's position follows the equation

$$x(t)=D(\omega)\cos[\omega t-\delta(\omega)] \tag{7}$$

where

$$\frac{D(\omega)}{A}=\frac{1}{(1+\tau^2\omega^2)^{1/2}} \quad \text{and} \quad \delta=\tan^{-1}(\tau\omega) \tag{8}$$

and $\tau=6\pi\eta a/k_{\mathrm{ot}}$.

In the scheme of detecting the particle motion mentioned above, the position of the particle is measured relative to the moving reference frame of the oscillating trap. One can make a straightforward transformation, $x(\omega)=A-x'(\omega)$, to convert the motion relative to the oscillating frame (denoted by x'), to the motion relative to the stationary laboratory frame

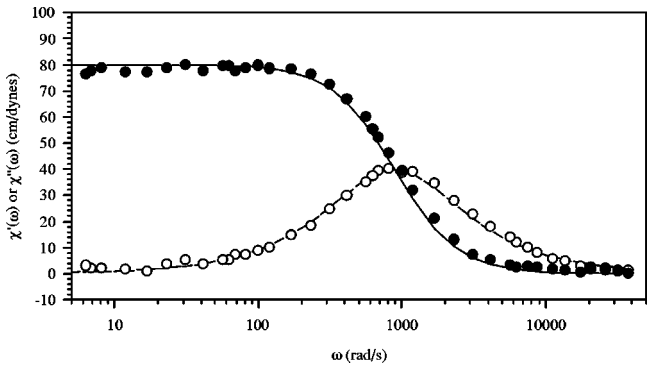

FIG. 3. Typical calibration data for the determination of the spring constant of an optical trap. The solid and dash lines indicate the real and imaginary parts of the response of a single damped harmonic oscillator given by Eq. (11), with $k_{\mathrm{ot}}=0.0125$ dyn/cm.

(denoted by x). In terms of the measured phase δ' and displacement D' of the particle in the moving frame, the displacement D and phase shift δ in laboratory frame are given by

$$D^2=D'^2-2AD\cos(\delta')+A^2, \tag{9}$$

$$\delta=\tan^{-1}\left(\frac{D'\sin(\delta')}{D'\cos(\delta')-A}\right). \tag{10}$$

The spring constant can be obtained by fitting Eq. (3), with $k_{\mathrm{ot2}}=0$, to the response obtained by the laboratory frame phase and displacement of the single particle in water [13]. Specifically,

$$\chi(\omega)=\frac{De^{i\delta}}{Ak_{\mathrm{ot}}}=\frac{1}{k_{\mathrm{ot}}}\left[\frac{1}{1+\tau^2\omega^2}+i\frac{\omega\tau}{1+\tau^2\omega^2}\right]. \tag{11}$$

A typical data set taken for a trapped particle in water at room temperature is shown in Fig. 3. Here $k_{\mathrm{ot}}=0.0125$ dyn/cm is obtained without adjustable parameters. Reports by others have found that the heating of the particle by optical tweezers, at the level of a few milliWatts of laser power, is negligible [16]. In the determination of trap spring constant we assume the viscosity of water around the particle to be the same as the viscosity at ambient temperature. We use the same procedure to determine the spring constant for each trap, and the values so obtained are used in the following experiments.

Trap spring constants so determined are checked against the power spectrum method [17] with a R2000 Rapid Systems Spectrum Analyzer for a stationary trap configuration similar to that described above. According to the fluctuation-dissipation theorem, Eq. (A9), the power spectrum of the position fluctuation of an isolated particle is

$$\langle x(\omega)x(0)\rangle=\frac{2k_BT}{\omega}\chi''(\omega). \tag{12}$$

Following Eq. (11) we see that the power spectrum density (PSD) can be written as

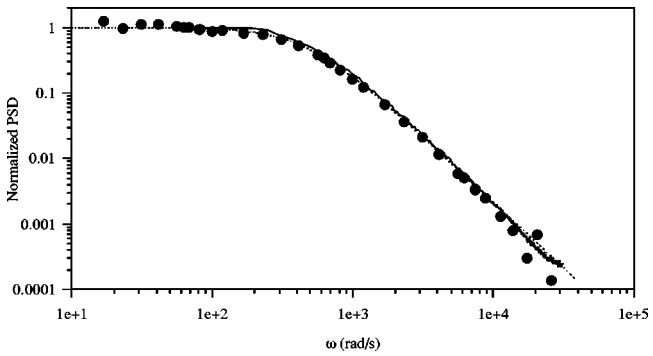

FIG. 4. The normalized power spectral density (PSD) versus frequency as a confidence check of the calibration of a spring constant. The solid circles are calculated according to $D\sin\delta/A\omega$ from the experimentally determined displacement and phase shift using the oscillating tweezers technique. The solid line is the experimentally determined normalized PSD. The dash line is calculated values of $1/(1+\tau^2\omega^2)$ with $\tau=6\pi\eta a/k_{\mathrm{ot}}$, with $k_{\mathrm{ot}}=0.0125$ dyn/cm.

$$\langle x(\omega)x(0)\rangle=\frac{2k_BT}{k_{\mathrm{ot}}}\frac{\tau}{1+\tau^2\omega^2}=\frac{2k_BT}{k_{\mathrm{ot}}}\frac{D(\omega)\sin[\delta(\omega)]}{A\omega}. \tag{13}$$

In Fig. 4, the solid circles are the experimentally determined $[D\sin(\delta)/A\omega]$, the solid line is the normalized PSD such that its asymptotic value at low frequency is 1. The dashed line is the calculated values of $1/(1+\tau^2\omega^2)$ with $\tau=6\pi\eta a/k_{\mathrm{ot}}$, and $k_{\mathrm{ot}}=0.0125$ dyn/cm. The fact that the dashed line fits so well to both the normalized PSD and the data obtained by the same particle in an oscillating trap, gives a confidence check to the calibration of a trap spring constant.

For the two-particle experiment, one particle is held in each of the tweezers and isolated in the manner described above. The oscillating trap (trap 1) is set into sinusoidal motion along the line connecting the particles' centers over a frequency range of $1<f<6000$ Hz while the second trap remains stationary at a distance R away. Since the second trap is stationary, the motion of the particle in the stationary trap is measured relative to stationary laboratory frame. The oscillation amplitude of trap 1 is kept at 20 nm, at least 20 times less than the minimum separation distance between the particles. The distance between the centers of the particles is determined by video image analysis with an accuracy of 20 nm. The particles are held at a distance of approximately 20 μm from the cover slip to avoid wall effects.

To test for possible optical interference between the traps, the particle from the stationary trap is removed, and the phase shift of the particle in the oscillating trap is measured as a function of the distance between the two traps. For trap separation distances greater than one-half of the particle radius, the measurements indicate that the empty trap has no significant effect on the motion of the first particle. Optical interference between the two tweezers when both the particles are in the traps is considered insignificant due to the following reasons. First, the particle's diameter is about three times the optical wavelength, therefore, the optical fields scattered off the particles are mostly in the forward direction.

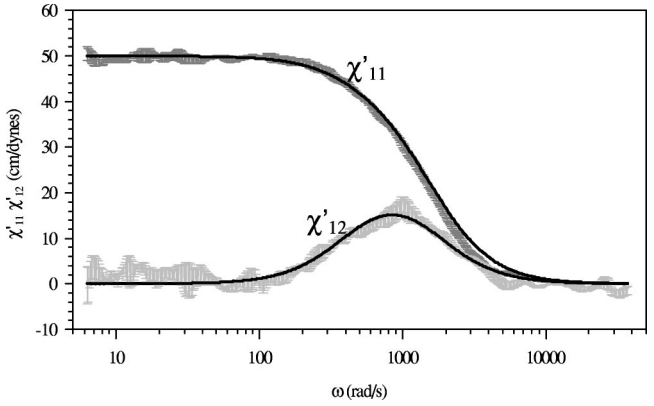

FIG. 5. The real part of the diagonal, $\chi'_{11}(\omega)$, and off-diagonal, $\chi'_{12}(\omega)$, components of the response tensor for two 1.6-μm silica particles in quadratic potential wells held at a distance $R=3.32a$ apart. The experimental data are shown with error bars. The solid lines are the real components of Eqs. (3) and (4).

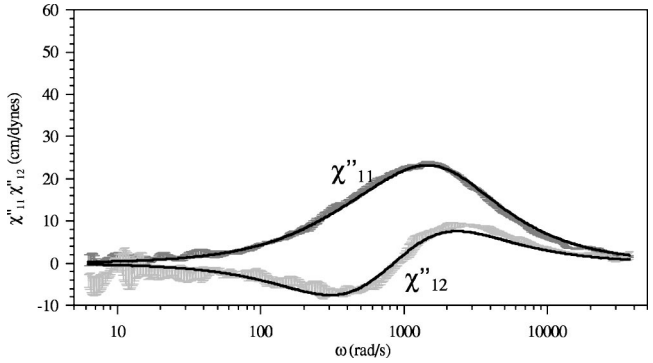

FIG. 6. The imaginary part of the diagonal, $\chi''_{11}(\omega)$, and off-diagonal, $\chi''_{12}(\omega)$, components of the response tensor for the same conditions as Fig. 5. The experimental data are shown with error bars. The solid lines are the imaginary components of Eqs. (3) and (4).

Indeed, the ratio of scattered light intensity in the forward direction to that of the perpendicular direction is more than 1000: 1 [18]. Second, since the two tweezers are formed by laser beams that are perpendicularly polarized to each other, only the first particle trapped by the laser beam polarized perpendicular to the line connecting the two particles can scatter light in the perpendicular direction, where the second particle is located. Thus, the optical interference at the second particle is negligible because the field scattered from the first particle is weak and polarized perpendicularly to the field that traps the particle. At the first particle, the magnitude of the optical interference between the trapping field and the second order scattered light is insignificant. Near field effects are negligible in this study, since the separation distances between the particles is always greater than one wavelength.

From the ratio of the motion in the stationary laboratory frame, $x_n(\omega)$, and the external driving force of the oscillating tweezers (sinusoidal perturbation) $F_1=Ak_{\mathrm{ot1}}$, (A is the amplitude of the oscillating trap), we obtain the elements of the response tensor $\chi_{11}(\omega)$ and $\chi_{21}(\omega)$ [15]. The phase shift, absent from the typical noise power spectrum measurements, provides a direct determination of both the real and imaginary parts of the response tensor.

The real and imaginary components of the elements of the response tensor, $\chi_{11}(\omega)$ and $\chi_{21}(\omega)=\chi_{12}(\omega)$, are shown in Figs. 5 and 6, respectively, for a separation distance of $2a/R=0.602$ with $k_{\mathrm{ot1}}=0.02$ dyn/cm and $\alpha=0.425$. The experimental data are averaged over three sets of measurements. The solid lines are the theoretical predictions of the response tensor from Eqs. (3) and (4), without adjustable parameters. The results compare very well for all the elements. The diagonal element χ_{22}, a linear combination of χ_{11} and χ_{12}, is not measured.

It is important to note, in Fig. 6, that $\chi''_{12}(\omega)$ is negative in a well-defined frequency region. The negative values of $\chi''_{12}(\omega)$ indicate a net energy gain of the particle in the stationary trap. The apparent energy gain of the second particle in this frequency range occurs at the cost of the extra dissipation of the particle in the oscillating trap. The fact that energy is shared between the two particles appeared as the pronounced dip in the cross-correlation functions of the particles as measured by Meiners and Quake [11].

Physically, the fact that $\chi''_{12}(\omega)$ is negative results from a negative phase lag between the oscillating trap and the particle in the stationary trap. This is most readily understood by considering a case at low frequencies, when the phase lag between the particle in the oscillating trap, and oscillating trap is near zero. At the time when $x_1=0$, the particle has a maximum velocity, resulting the transmission of maximum force to the second particle at the speed of sound. As a result, the second particle is moved toward $x_2=x_{2\,\mathrm{max}}$. Similarly, when $x_1=x_{1\,\mathrm{max}}$, the particle has a zero velocity, resulting in no force on the second particle such that the second particle relaxes back to $x_2=0$. Thus the second particle is $-90°$ out of phase with the driving force at very low frequencies. At larger frequencies, as the viscous damping effects become more important, the phase shift increases and becomes positive above a characteristic crossover frequency.

It is worth noting that the zero crossover point in $\chi''_{12}(\omega)$ corresponds to a maximum in $\chi'_{12}(\omega)$. The frequency at which the crossover occurs is $\omega_c=\sqrt{s_+s_-}$, and the maximum in the real part of the off-diagonal component of the response tensor is,

$$\chi'_{12}(\omega_c)=\frac{-\epsilon}{k_{\mathrm{ot1}}\tau(s_++s_-)}=\frac{3a}{2Rk_{\mathrm{ot1}}(1+\alpha)}. \qquad (14)$$

Measurements are taken at several particle separations to test the dependence of $\chi'_{12}(\omega_c)$ on the separation distance R. Figure 7 shows the experimental values of $\chi'_{12}(\omega_c)$ and the theoretical prediction given in Eq. (14). The data point at $2a/R=0.692$ is not in statistical agreement with the prediction. Including higher order terms in $2a/R$ in the Oseen Tensor does not account for the discrepancy. However, the discrepancy could arise from the repulsive electrostatic force between the two charged colloidal particles at close proximity, as explained below. The digital images of the two particles are found to be slightly farther apart than the spacing between the centers of the two traps when the two particles

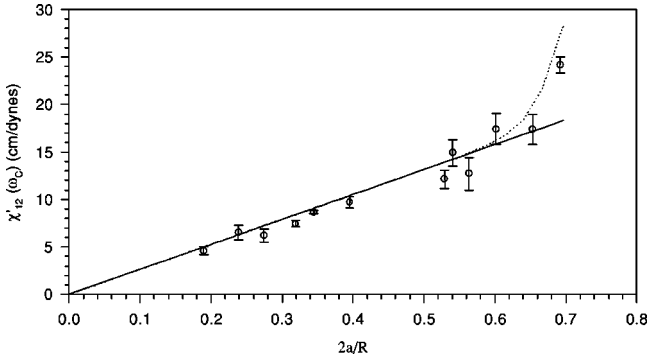

FIG. 7. The maximum values of χ'_{12} versus the normalized interparticle spacing, $2a/R$. The solid line is the prediction given by, Eq. (14). The dashed line is given by Eq. (14) with the effective spring constants replacing k_{ot1} and k_{ot2}.

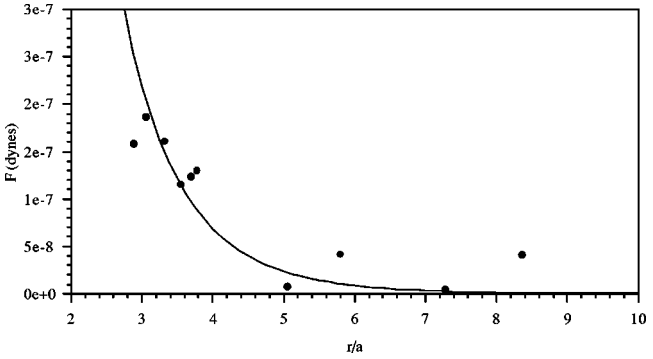

FIG. 8. Static repulsive force versus separation distance. The points indicate forces calculated by Eq. (15) from the measured equilibrium distance of the particle from the center of the oscillating trap. The line indicates a fit to the DLVO theory, with an ion concentration of 10^{-7} M, and a surface charge of $Z=1000e$.

are brought to within a couple of micrometers of each other. When a particle is away from the center of the trap it experiences a progressively weaker effective spring constant because the potential well formed by the trap is Gaussian rather than truly parabolic. In a Gaussian potential, the restoring force of the optical trap is given by

$$F=-k_{ot}xe^{-x^2/a^2}, \tag{15}$$

where x is the distance between the center of the particle and the center of the optical trap, and the width of the trap is taken to be approximately of the particle size ($a=0.8\ \mu$m) [13]. The dynamics of a small oscillation around any point in the Gaussian potential well can be calculated by considering the oscillation under a local, effective spring constant

$$k_{ot\,eff}=k_{ot}e^{-x_{eq}^2/a^2}\left[1-2\frac{x_{eq}^2}{a^2}\right], \tag{16}$$

where x_{eq} is the equilibrium position of the particle relative to the center of the optical trap.

The position of each particle relative to the center of a trap can be determined to within an accuracy of about 20 nm by comparing the video images of the particle with and without the presence of a second particle nearby. From the position of the particle relative to the center of the oscillating trap, the static force at each separation distance can be obtained by Eq. (15). As shown in Fig. 8, the static force on the particle in the oscillating trap compares well to the predictions of the Derjaguin, Landau, Verwey, and Overbeek (DLVO) theory for electrostatic repulsion between two colloidal particles [19]. The ionic strength calculated from the electrostatic repulsion is approximately 10^{-7} M, within the limits of which can be present in distilled water, and the effective surface charge is found to be $1000e$. Using the fitting force function and Eq. 15, we calculate the equilibrium positions for each of the particle pair. The effective spring constants for each particle at these positions are then determined from Eq. (16). The effective spring constants are used to calculate the expected response functions by Eq. (14). The dashed line in Fig. 7, is given by Eq. (14) with the effective spring constants replacing k_{ot1} and k_{ot2}. The good agreement between the data and the theoretical prediction indicates that electrostatic forces between the two particles are likely the cause for the discrepancy between the data and Eq. (14) in its original form.

V. SUMMARY

As a first step to understand the interactions between particles in complex fluids, we have examined the correlated motions of two hydrodynamically coupled colloidal particles confined in separate quadratic potential wells in water. Solving the coupled equations of motion for the particles, and calculating the autocorrelation and cross-correlation functions of the particles' motion, lead to the description of the mechanical response tensor of the coupled system. The experiments to determine the elements of the response tensor are carried out by using two optical tweezers, each of which holds a micron-sized colloidal particle in the potential well created by the tweezers. By oscillating one of tweezers, and thus the particle in it, we have measured the in-phase and out-of-phase motion of each of the particles by the lock-in detection method. From the motions of the particles, we have determined the mechanical response functions for the coupled system as a function of frequency. The theoretical model and the experimental results agree very well over a frequency range between 1 and 6000 Hz. Since the trap potential well is Gaussian, rather than truly parabolic, the response function χ_{12} can be significantly affected by the electrostatic repulsion between the two particles when the two particles are in close proximity. Measuring the correlated motion in the frequency domain allows for a simple physical interpretation of the in-phase and out-of-phase motions of the particles. The study presented in this paper demonstrates that it is possible to directly measure the transmission of hydrodynamic forces across a viscous medium in a microscopic environment and in a confined geometry. The new challenge arises with the possibilities of extending this approach for complex fluids that are viscoelastic and/or heterogeneous.

ACKNOWLEDGMENTS

The work was supported in part by a grant from the National Science Foundation, CTS-9805887, and a grant from

Alcoa. L. A. H. is grateful for the assistance from S. J. Parmley and J. C. Daghlian in learning the experiment.

APPENDIX: CALCULATION OF THE RESPONSE TENSOR

To solve the coupled differential equations of motion we first rewrite Eq. (1) as

$$\tau\dot{x}_1(t) = -x_1(t) + \frac{f_1(t)}{k_{ot1}} - \epsilon\alpha x_2(t) + \epsilon\frac{f_2(t)}{k_{ot1}},$$

$$\tau\dot{x}_2(t) = -\epsilon x_1(t) + \epsilon\frac{f_1(t)}{k_{ot1}} - \alpha x_2(t) + \frac{f_2(t)}{k_{ot1}}, \quad \text{(A1)}$$

where $\alpha = k_{ot2}/k_{ot1}$, $\epsilon = H_{12}/H_{11}$, and $\tau = 1/(k_{ot1}H_{11})$.

We then take the Laplace transform of Eq. (A1) with $x(s) = \int_0^\infty x(t)e^{-st}$.

To construct the autocorrelation and cross-correlation functions by taking the ensemble average of $x_m(s)$ and $x_n(t=0)$, the results show below

$$\langle x_1(s)x_1(0)\rangle = \frac{k_BT}{k_{ot1}\tau}\left[\frac{\alpha+\tau s}{(s-s_-)(s-s_+)}\right], \quad \text{(A2)}$$

$$\langle x_2(s)x_2(0)\rangle = \frac{k_BT}{\alpha k_{ot1}\tau}\left[\frac{1+\tau s}{(s-s_-)(s-s_+)}\right], \quad \text{(A3)}$$

$$\langle x_2(s)x_1(0)\rangle = \langle x_1(s)x_2(0)\rangle = \frac{-\epsilon k_BT}{k_{ot1}\tau}\left[\frac{1}{(s-s_-)(s-s_+)}\right], \quad \text{(A4)}$$

where k_B is Boltzmann's constant, and T is the absolute temperature, k_{otn} is the spring constant of the nth harmonic well, and δ_{nm} is the Kronecker δ function, and $s_\pm$ are as defined in Eq. (6). Note that the relation

$$\langle x_n(0)x_m(0)\rangle = \frac{k_BT}{k_{otn}}\delta_{nm}, \quad \text{(A5)}$$

is used in arriving to the results given in Eqs. (A2)–(A4).

The autocorrelation and cross-correlation functions in time domain are obtained by the inverse Laplace transformation $x(t) = [1/(2\pi i)]\int_{\gamma+i\infty}^{\gamma-i\infty} x(s)e^{st}$ of Eqs. (A2)–(A4).

$$\langle x_1(t)x_1(0)\rangle = \frac{k_BT}{k_{ot1}\tau(s_+-s_-)}[(\alpha+\tau s_+)e^{s+t} - (\alpha+\tau s_-)e^{s-t}], \quad \text{(A6)}$$

$$\langle x_2(t)x_2(0)\rangle = \frac{k_BT}{\alpha k_{ot1}\tau(s_+-s_-)}[(1+\tau s_+)e^{s+t} - (1+\tau s_-)e^{s-t}], \quad \text{(A7)}$$

$$\langle x_2(t)x_1(0)\rangle = \langle x_1(t)x_2(0)\rangle = -\frac{\epsilon k_BT}{k_{ot1}\tau(s_+-s_-)} \times [e^{s+t} - e^{s-t}]. \quad \text{(A8)}$$

Note the resulting Eqs. (A6)–(A8) are consistent with Meiners and Quake's calculations [11].

The imaginary part of the response function is related to the correlations by the fluctuation-dissipation theorem [15]

$$\chi''_{nm}(\omega) = \frac{\omega}{2k_BT}\langle x_n(\omega)x_m(0)\rangle, \quad \text{(A9)}$$

where $\langle x_n(\omega)x_m(0)\rangle$ is the Fourier transform of $\langle x_n(t)x_m(0)\rangle$. The real part of the response function is determined from the imaginary part of the response function by the Kramers-Kronig relation [15]

$$\chi'_{nm}(\omega) = P\int_{-\infty}^{\infty}\frac{d\omega'}{\pi}\frac{\chi''_{nm}(\omega')}{\omega'-\omega}, \quad \text{(A10)}$$

where P signifies the principle part. The components of the response tensor χ_{nm} are shown as Eqs. (3)–(5) in the main text.

[1] T. G. Mason and D. A. Weitz, Phys. Rev. Lett. **75**, 2770 (1995).
[2] T. G. Mason *et al.*, Phys. Rev. Lett. **79**, 3282 (1997).
[3] F. Gittes *et al.*, Phys. Rev. Lett. **79**, 3286 (1997).
[4] E. Helfer *et al.*, Phys. Rev. Lett. **85**, 457 (2000).
[5] J. C. Crocker *et al.*, Phys. Rev. Lett. **85**, 888 (2000).
[6] L. A. Hough and H. D. Ou-Yang, J. Nanopart. Res. **1**, 495 (1999).
[7] A. R. Bausch *et al.*, Biophys. J. **75**, 2038 (1998).
[8] F. Ziemann, J. Radler, and E. Sackmann, Biophys. J. **66**, 2210 (1994).
[9] M. Yanai *et al.*, Am. J. Physiol. **277**, C432 (1999).
[10] A. J. Levine, T. C. Lubensky, Phys. Rev. Lett. **85**, 1774 (2000).
[11] J-C Meiners and S. R. Quake, Phys. Rev. Lett. **82**, 2211 (1999).
[12] M. T. Valentine, L. E. Dewalt, and H. D. Ou-Yang, J. Phys.: Condens. Matter **8**, 8477 (1996).
[13] H. D. Ou-Yang, in *Polymer-Colloid Interactions: From Fundamentals To Practice*, edited by P. Dubin and R. Fainato (Wiley, New York, 1999), Chap. 15, pp. 385–405.
[14] M. Doi and S. F. Edwards, *The Theory of Polymer Dynamics* (Clarendon, Oxford, 1986).
[15] P. M. Chaikin and T. C. Lubensky, *Principles of Condensed Matter Physics* (Cambridge University Press, Cambridge, 1995).
[16] T. Lin, G. J. Sonek, M. W. Berns, and B. J. Thromberg, Biophys. J. **71**, 2158 (1996).
[17] F. Gittes and G. F. Schmidt, Methods Cell Biol. **55**, 129 (1998).
[18] M. Born and E. Wolf, *Principles of Optics*, 4th ed. (Cambridge University Press, Cambridge, 1970).
[19] J. C. Crocker and D. G. Grier, Phys. Rev. Lett. **73**, 352 (1994).